Influence of hydromechanical heterogeneities of fault zones on earthquake ruptures

F. Cappa

Geophysical Journal International

Geophys. J. Int. (2011) **185,** 1049–1058 doi: 10.1111/j.1365-246X.2011.04994.x

Influence of hydromechanical heterogeneities of fault zones on earthquake ruptures

Frédéric Cappa

GeoAzur (UMR6526), University of Nice Sophia-Antipolis, Côte d'Azur Observatory, F-06560 Sophia-Antipolis, France.
E-mail: frederic.cappa@geoazur.unice.fr

Accepted 2011 February 18. Received 2011 February 18; in original form 2010 May 14

SUMMARY

Fluid pressurization, a possible mechanism of fault weakening, exerts a critical control on earthquake rupture in the upper crust. One cause for this control is the presence of high fluid pressures inside the fault zone. However, the precise mechanisms relating high fluid pressures and fault rupture remain unclear. Here, we use 2-D hydromechanical models to show that effective stress changes induced by a transient pulse of fluid pressure along a fault zone with spatially variable material properties—conditions that are representative of natural faults—can be sufficient to produce large slip in the fault core, and fracturing in the surrounding damage volume. Rupture properties outside the limited source region are examined for ranges of values of the degree of material contrast across the fault. Our results indicate that the slip dimension is highly influenced by the contrasts of permeability and rigidity across the fault zone components, from the fault core through the various subzones of the fractured damage zone and to the less fractured host rock. Moreover, high fluid pressures may also develop locally off the narrow fault core, preferentially into the more permeable and less rigid parts of the damage zone, where the deformation is plastic, highlighting a possible mechanism for off-fault rupture. Finally, on faults with hydromechanical heterogeneities at the scale of the internal structure, the fluid pressure and rupture are highly asymmetric with propagation in a preferred direction, that is the more permeable and compliant material of the fault zones.

Key words: Permeability and porosity; Fracture and flow; Fault zone rheology; Earthquake dynamics; Dynamics and mechanics of faulting; Mechanics, theory, and modelling.

1 INTRODUCTION

Large earthquakes (M > 6) typically occur at ∼8–15 km depths in the Earth's crust (Scholz 2002); depths where fluids may be present as evidenced by geophysical observations in several seismogenic zones (Becken *et al.* 2008; Wannamaker *et al.* 2009). These fluids may have significant effects on fault mechanics and earthquake rupture (Sibson 1973; Scholz 2002; Wibberley & Shimamoto 2005; Rice 2006). Under some conditions, fluids can facilitate slip on faults at stress levels lower than those required under dry conditions. When fluids are present in fault zones, they can escape or accumulate depending on the internal structure and the hydraulic properties of the fault zone. If the fluid pressure in the fault principal slip zone (PSZ) and in the fractured rock volume around it increases, the effective normal stress across the fault will decrease; this effect will in turn reduce the fault strength according to the Coulomb failure criterion (Sibson 1973; Scholz 2002; Wibberley & Shimamoto 2005; Rice 2006). Although pressurized fluids (i.e. suprahydrostatic overpressures) are now understood to weaken faults, a central difficulty in evaluating the relationship between fluid pressure and fault slip lies in the variations in material properties across the fault zone. The juxtaposition of rocks with dissimilar properties is a general feature of fault zones in a variety of contexts and scales; especially, at the scale of the internal structure of a fault zone, where heterogeneity of properties associated with rock damage is significant (Dor *et al.* 2006a). Geological observations have shown that the hydromechanical properties across the faults vary asymmetrically (Fig. 1), and that the fractured damage zone around the fault core is the main path for fluids (Cappa *et al.* 2007; Guglielmi *et al.* 2008; Gudmundsson *et al.* 2010). For instance, this configuration is known at the San Andreas Fault (SAF) in Parkfield where the fault zone is located at the boundary between the Great Valley sediments and the Franciscan Complex to the east and the Salinian basement to the west (Hickman *et al.* 2004; Fulton & Saffer 2009). Several geophysical observations in the Parkfield region have shown that the Salinian basement is less permeable than rocks to the east of the SAF (Becken *et al.* 2008; Fulton & Saffer 2009). Moreover, others geological and seismological studies along the SAF, Punchbowl and San Jacinto faults in southern California have shown asymmetry in the damage patterns of fault zone rocks, with one side having considerably more damage than the other (Dor *et al.* 2005; Lewis *et al.* 2005).

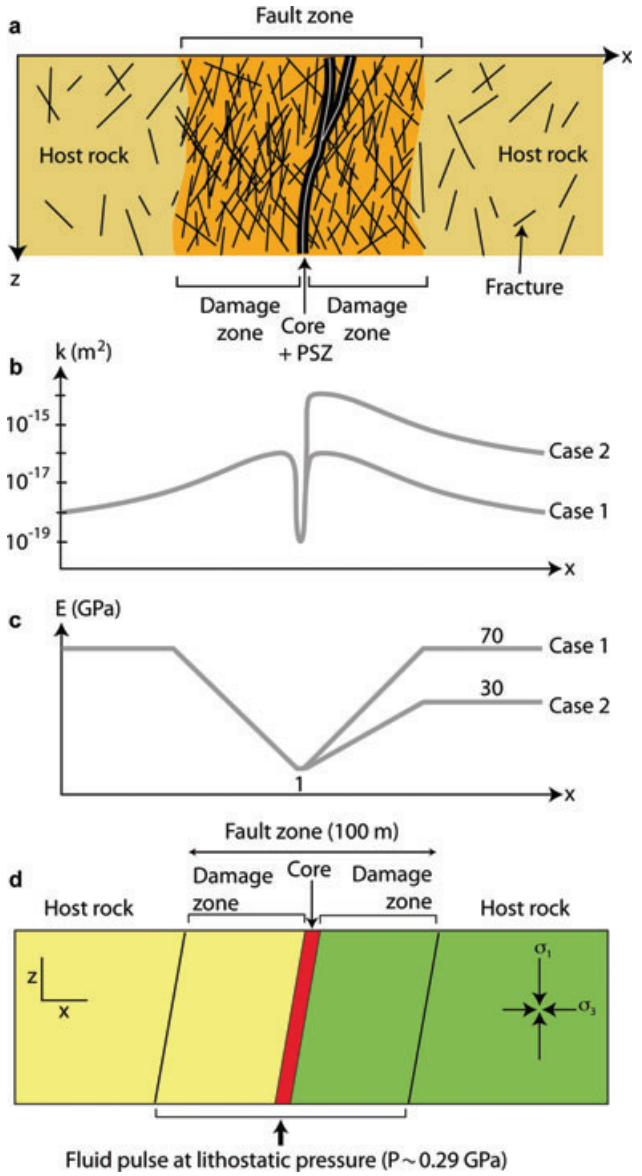

Figure 1. Model of fault zone structure and properties. (a) Schematic diagram of the structure across a fault zone illustrating relationships between the principal slip zone (PSZ in grey), fault core (in black) and damage zones (in orange); and model of the distribution of permeability in (b) and Young's modulus in (c). In the damage zone, the fracture density decreases with distance to a regional background level. (d) Model of the hydromechanical interaction between the fault zone elements, that is, from the fault core through the damage zone and to the host rock. The fault dip angle is of 80° towards the right side of the model. The fault core is represented by a thin zone (Young's modulus E = 1 GPa, Poisson ratio $\nu = 0.3$, density $\rho = 3000$ kg m^{-3}, cohesion $c = 0$, static friction coefficient $\mu_s = 0.4$, zero stress porosity $\phi_0 = 0.1$, zero stress permeability $k_0 = 10^{-17}$ m^2). The PSZ is represented by an interface with a Coulomb friction law inside the fault core. The damage zone is divided in several parallel subzones with properties varying gradually as seen in (b) and (c). In case 1, the properties are symmetrically distributed on each sides of the fault core, whereas in case 2, the right side (in green) of the fault core is more permeable and less rigid than the left side (in yellow).

Earthquake slip along faults in the upper continental crust generally occurs along an extremely localized boundary between materials of different physical properties, such as gouge lying between the fault core and the damage zone (Vermilye & Scholz 1998; Sibson 2003; Wilson *et al.* 2003; Wibberley & Shimamoto 2003; Faulkner *et al.* 2006; Mitchell & Faulkner 2009; Sone & Shimamoto 2009). The PSZ is often less than 10 cm and, in many cases, less than 1 cm in thickness, and can accomodate large finite displacements (>1 km; Sibson 2003). Strong contrasts of seismic velocity, permeability and rigidity have been measured in the fault zone components and in the surrounding host rocks (Faulkner & Rutter 1998; Wibberley & Shimamoto 2003; Gudmundsson 2004; Faulkner *et al.* 2006; Cappa *et al.* 2007; Guglielmi *et al.* 2008; Gudmundsson *et al.* 2010). These measurements revealed that the permeability and Young's modulus of a fault zone vary significantly with distance from the PSZ itself, that is, from the core through the fractured damage zone and to the less fractured host rock. The fractures generally make the damage zone more permeable than the fault core, and the gouge makes the core less rigid than the damage zone.

Physics of earthquake rupture received considerable attention over the last 20 years, especially in the understanding of dynamic rupture propagation, and, more recently, on the coseismic plastic strain off the fault. Previous research has focused on faults with either uniform materials adjacent to the fault surface (Andrews 2002, 2005; Rice 2006; Templeton & Rice 2008), with material properties varying symmetrically on both sides of the fault (Noda & Shimamoto 2005; Cappa 2009), or with dissimilar materials across the fault (Ben-Zion & Shi 2005; Shi & Ben-Zion 2006; Brietzke & Ben-Zion 2006). Others works by Rudnicki & Rice (2006) and Dunham & Rice (2008) have studied the effect of pore pressure induced by a dynamically propagating slip on a fault zone between dissimilar poroelastic materials, especially permeability. Later, Viesca *et al.* (2008) have extended these works and studied how the fault undrained behaviour (i.e. no fluid diffusion occurs) affects the rupture dynamics and coseismic off-fault plasticity. In contrast with those researches, we examine here the effect of pore pressure diffusion induced by a high-pressure source rather than a dynamically propagating rupture on the fault slip and plastic strain off the fault. We focus on the drained behaviour of a fault zone with contrasted hydromechanical properties varying progressively from the core zone through the damage zone and to the intact host rock. A systematic parameter-space study is conducted with different values of permeability and Young's modulus to cover effects associated with different degrees of material contrast across the fault. Thus, we address in this paper: (1) the importance of the contrast in hydraulic and mechanical properties on the hydromechanical and rupture behaviour of a fault zone when the fluid pressure increases, and (2) the following question: where does off-fault plastic deformation develop, and how such deformation affect the fault behaviour? The results show that for broad ranges of realistic parameters the fluid pressure and rupture in and off the slip zone are sensitive to the material contrast, especially permeability, and evolve with a preferred propagation direction, that is the more permeable and less rigid side of the fault zone.

2 NUMERICAL MODEL

To take into account the difference in permeability and rigidity between the fault zone components and the host rocks, and to examine how these properties influence fault rupture during fluid pressurization, we carried out 2-D hydromechanical numerical experiments of fluid flow and deformation along a near-vertical fault zone composed of elasto-plastic materials (see Appendix). The model extends vertically down to 10 km, and horizontally far enough from

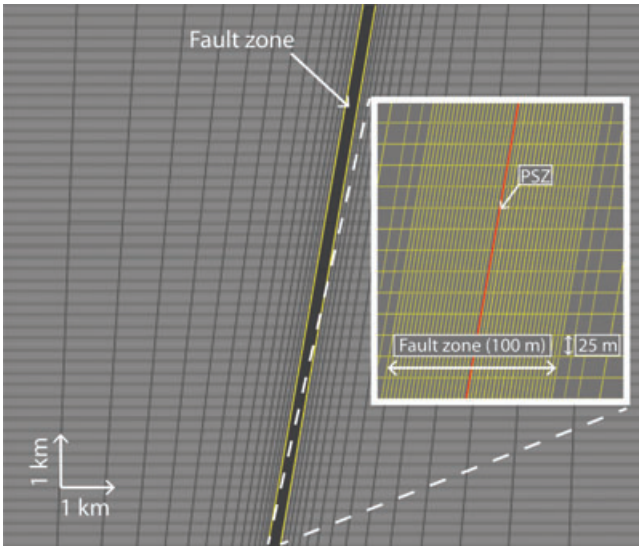

Figure 2. Close-up view of the mesh inside the fault zone. The red line corresponds to the interface representing the principal slip zone (PSZ) inside the fault core. Inside the fault zone, each element is 5 m wide and 25 m high.

the source region where we imposed a pulse of fluid pressure corresponding to the lithostatic pressure at the base of the fault (Figs 1d and 2). The fault is distinctly discretized as a 100 m thick zone with a thin core zone embedded in a damage zone (Fig. 2). The PSZ is represented by an interface with a Coulomb friction law (static friction coefficient, $\mu_s = 0.4$). This interface is surrounded by the fault core, whose Young's modulus is taken as 1 GPa as measured in the laboratory (Gudmundsson 2004). In the model, the damage zone is composed of multiple, parallel zones, each of which exhibiting different hydromechanical characteristics reflecting the heterogeneity of fracture density and properties as presented in Fig. 1. The surrounding crust is considered as less fractured and composed of different rocks on both sides of the fault zone. We assume that the region with the higher permeability and the lower rigidity is on the right side of the fault core. In our study, we carried out several numerical experiments using variable permeability and Young's modulus architecture for the fault zone and the crust (Figs 1b and c, and 7). A difference of one to several orders of magnitude in material properties was analysed. This difference is consistent with measurements on exhumed faults, on which earthquakes occurred many decades/centuries years ago at seismogenic depths and are now exposed at the surface (Faulkner & Rutter 1998). We computed the fluid pressure and flow according to a diffusion equation (see Appendix) with spatially variable hydraulic parameters. We assumed a difference of two orders of magnitude between the initial values of permeability and porosity near the ground surface and the initial values at the base of the seismogenic crust (Faulkner & Rutter 1998). In the simulations, we also assume that the permeability and porosity vary with the total volumetric strain (see Appendix). The initial fluid pressure and stress conditions are illustrated in Fig. 3. Here, we assume an initial hydrostatic fluid pressure and an extensional stress regime with $\sigma_H = 0.75\ \sigma_V$. To distinguish the effects of fluid pressure from those of friction, we assume a constant μ_s to make fluid pressurization the only source of fault weakening in the model.

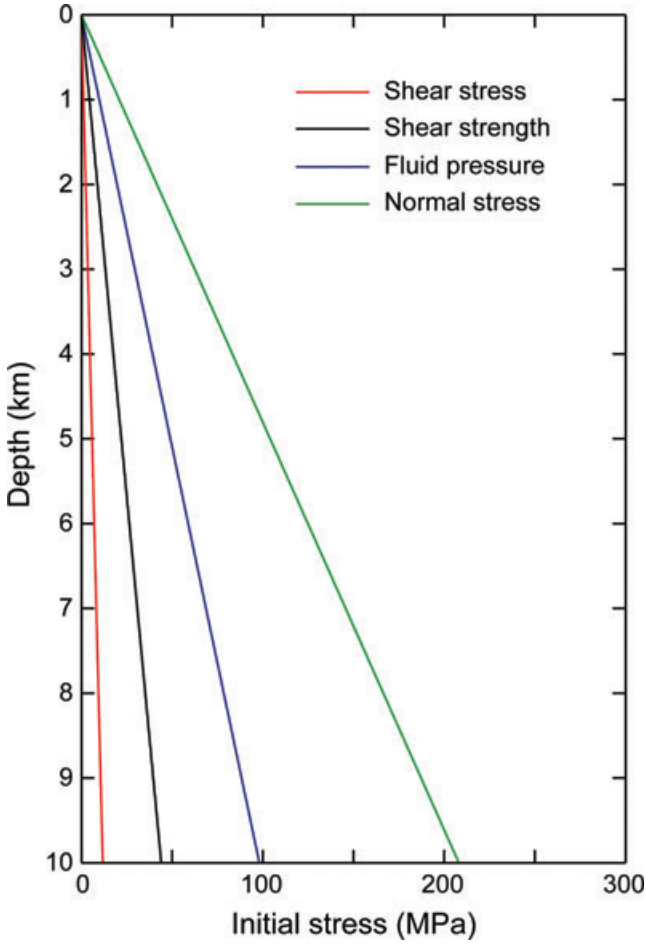

Figure 3. Initial fluid pressure and stress distribution with depth.

3 RESULTS

3.1 Hydraulic and rupture behaviour in a fault zone with dissimilar hydromechanical properties

To provide a context for the systematic parameter-space study presented in the next Section 3.2, we first discuss results for fluid flow and ruptures in the case of material properties varying symmetrically on both sides of the fault, and then for a difference of two orders of magnitude (cases 1 and 2 in Figs 1b and c). The latter is a general feature of fault zone heterogeneity. As shown in Figs 4 and 5, the sudden loading from the high-pressure source initiates a pressure pulse that propagates along the fault zone initially at hydrostatic fluid pressure. Indeed, the pressure front moves up the fault zone preferentially into the more permeable side of the damage zone (Fig. 4a). This evolution is a consequence of the initial heterogeneity of hydraulic properties and the strain dependent-permeability and porosity. The more permeable part of the damage zone is more prone to pressurization than the less permeable part because fluids can flow more easily and overpressures can be relieved more effectively. Consequently, in the more permeable side of the fault, the strength is reduced, deformation is increased and becomes plastic near the limited source region where local high stresses and strains develop in response to the pressurization (Figs 4b, 5 and 6). This induces a maximum increase in fault permeability up to two orders of magnitude (Fig. 4c). Thus, our results show that the plastic deformation is preferentially increased in the more

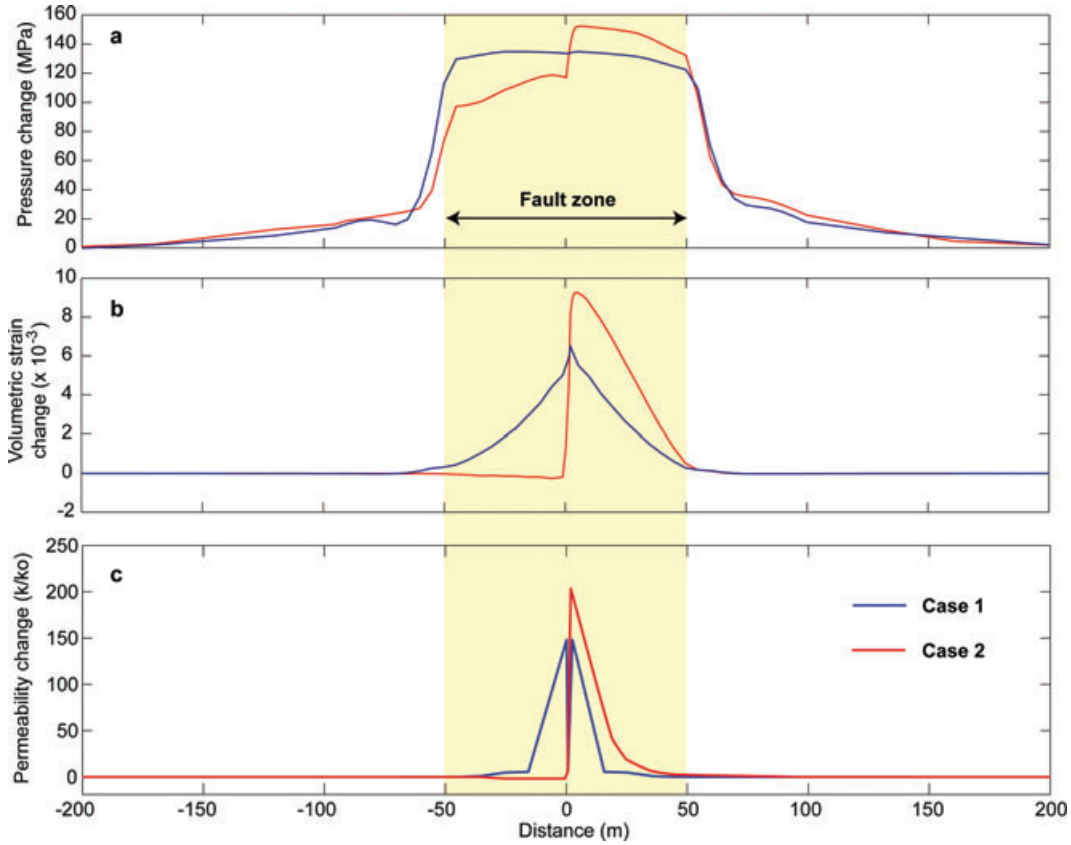

Figure 4. Results of modelling when fault slip and plastic strain stop varying (this corresponds to the simulated time $t = 1.5$ d). Horizontal profiles of change in fluid pressure in (a), volumetric strain in (b), and permeability in (c). Profiles are perpendicular to the fault zone (located at $x = 0$) near the source region at $z = 9.975$ km. Blue lines correspond to the model case 1, whereas red lines correspond to the model case 2. Note that the distribution of pressure, strain and permeability changes are nearly the same on the two sides of the fault core for the uniform model (case 1), whereas important differences emerge for the non-uniform model (case 2).

permeable and less rigid side of the fault zone (Fig. 6) where the effective normal stress is strongly reduced. This means that the rupture is distributed in a zone of several metres around the fault core, and does not solely occur along the PSZ. The largest amount of plastic strain are located near the high-pressure source region. The extent of the zone of plastic strain decreases with increasing the material contrast.

Fig. 4 further shows that the fluid pressure peak in the more permeable side of the fault zone is observed nearby the PSZ in the model where the contrast of permeability is the highest. This result indicates that fluid flows toward the PSZ from the pressure peak in the damage zone, following the pressure gradient. Thus, the amount of fluid pressurization, and hence slip along the PSZ and deformation in the damage zone are mainly controlled by the higher permeability and less rigid side of the fault.

Inside the fault core, high fluid pressures produce a localized weak zone with a lowered effective normal stress, an increased shear stress and an increased volumetric strain consisting in an expansion (i.e. dilatation) which is accompanied by an increase in porosity, with a corresponding increase in permeability (Figs 4 and 5). The largest variations in stress and strain are obtained for the fault zone having the largest contrast in hydromechanical properties (case 2). In all cases, the hydromechanical effect induces slip along the PSZ in the fault core. The larger slip is obtained for case 2 in which slip is about 2 m and distributed along a 1.2 km long active shear zone from the source region (Fig. 5d). In case 1, slip and shear zone length are lower (by a factor of $\sim$1.7). In the two simulated cases, the results suggest that fault slip is controlled primarily by changes in the effective normal stress.

3.2 Parameter-space study and signatures of the bimaterial effect

We conducted a systematic parameter-space study to estimate the impact of the degree of material properties contrast on the magnitude of slip and plastic strain, as well as the slip length along the PSZ and the ruptured area in the damage zone; thus, we can quantify the degree of asymmetry of rupture for a broad range of realistic conditions. The degree of material contrast $\gamma \geq 0$ across the slip zone is defined as $\gamma = P_1/P_2 - 1$ where P_1 denoting the material properties above the interface and P_2 the material below when the effect of rigidity is assessed [i.e. P_1 is fixed as in the case 1 (Fig. 1) with a maximum value of 70 GPa, whereas P_2 is varied for different maximum values comprised between 10 and 70 GPa; consequently, γ ranges from 0 to 6]. When the effect of permeability is estimated, P_1 denotes the material below the interface, and P_2 the material above [i.e. P_2 is fixed as in the case 1 (Fig. 1) with a minimum value of 1×10^{-18} m^2, whereas P_1 is varied for different minimum values comprised between 1×10^{-18} and 1×10^{-14} m^2; consequently, γ ranges from 0 to 10^4). Fault slip and plastic strain generated for the different sets of parameters are summarized in Fig. 7. The material contrast tends to produce highly asymmetric ruptures, which develop larger slip and plastic strain in the zone of higher

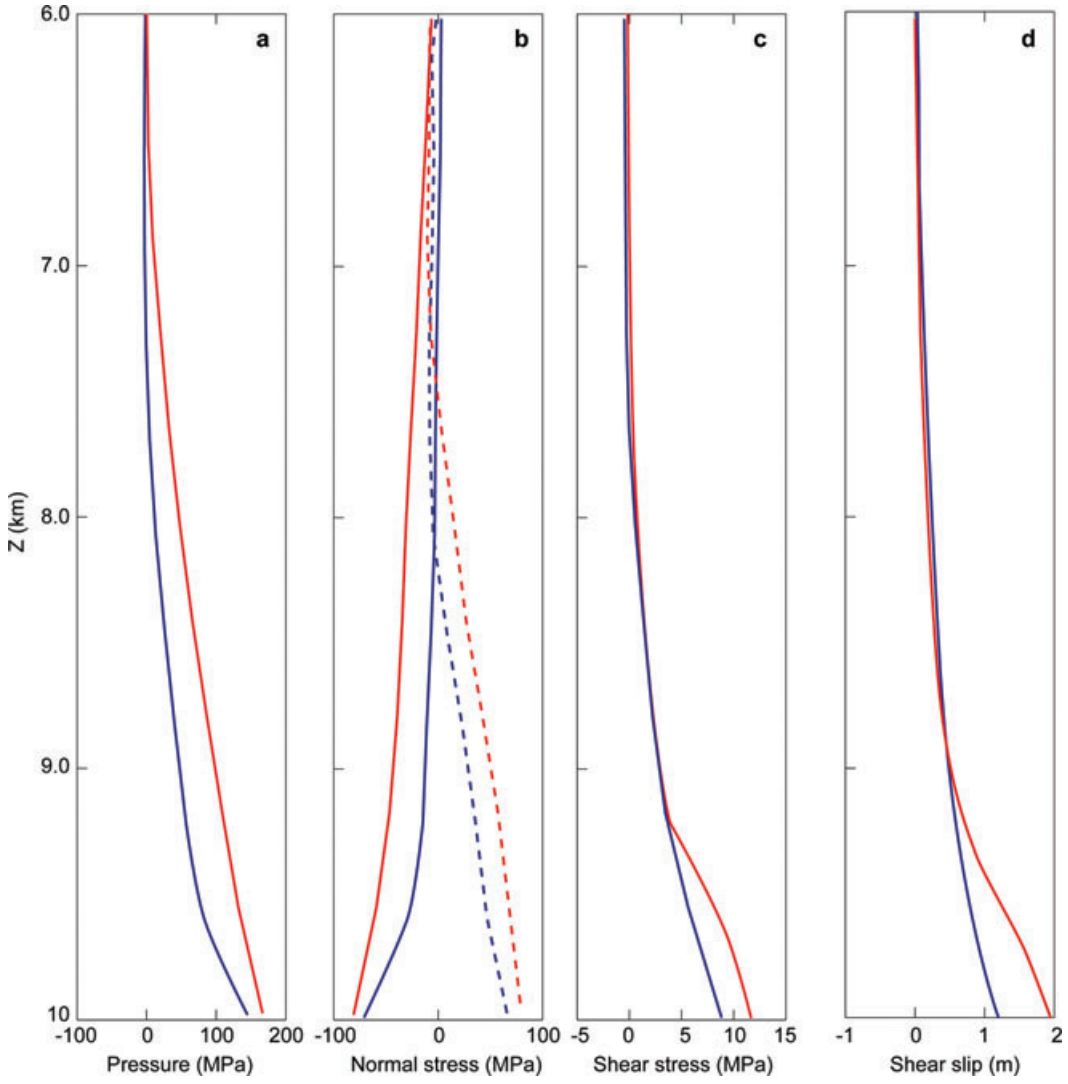

Figure 5. Vertical profiles of change in fluid pressure in (a), effective (solid lines) and total (dashed lines) normal stress in (b), shear stress in (c), and slip in (d) along the PSZ inside the fault core ($t = 1.5$ d). Blue lines correspond to the model case 1, whereas red lines correspond to the model case 2. Results indicate that the pore pressure rise induces a lowering of effective stress normal to the fault plane of several tens of MPa, but only an increase in shear stress of a few MPa. This means that failure is mainly related to the lowering of effective stress. In the overpressurized zone, the total stress normal to the fault plane is increased by several tens of MPa as a result of poroelastic stresses.

permeability and lower rigidity, and decay in the opposite direction (Figs 7a and b). Ruptures show varying degrees of asymmetry in slip length along the PSZ, and ruptured area in the damage zone off the PSZ (Figs 7c and d). Results indicated that when the degree of material contrast is increased, the amount of slip along the PSZ and plastic strain off the PSZ, within the damage zone, increase and the rupture asymmetry becomes more pronounced. The most prominent asymmetry is found for permeability contrasts higher than 10, and rigidity contrasts greater than four. The phase diagrams presented in Fig. 7 also show that the effect of the rigidity contrast becomes more pronounced for permeability contrasts higher than 10. Fig. 7(c) show that the slip length is higher when the rigidity contrast is small ($\gamma < 1$), and the permeability contrast is greater than 10. In contrast, for a small rigidity contrast, the ruptured area in the damage zone is higher for a permeability contrast less than 10. Thus, the slip propagation distance from the source region is higher when the extent of off-fault plastic strain is asymmetric.

In summary, the mechanism is controlled by the increasing fluid pressure that produces a stronger reduction in effective normal stress in the more compliant and permeable side of the fault where the rupture is more pronounced. The main signature of the bimaterial effect highlighted in this study is the highly asymmetric off-fault plastic strain, and increased slip associated with the permeability and rigidity contrast. In these simulations, the slip propagation distance and the ruptured area in the fault damage zone are less significantly affected by the material contrast.

4 DISCUSSION

4.1 Influence of fault zone heterogeneity on rupture

The difference in the results is due both to the contrast in initial hydromechanical properties among the fault zone components and also to the variations in hydraulic properties with volumetric strain, modulated by distribution of fluid pressure and stress. This study illustrates the effect of the contrasts in elastic and hydraulic properties in the various subzones of a fault on the hydromechanical

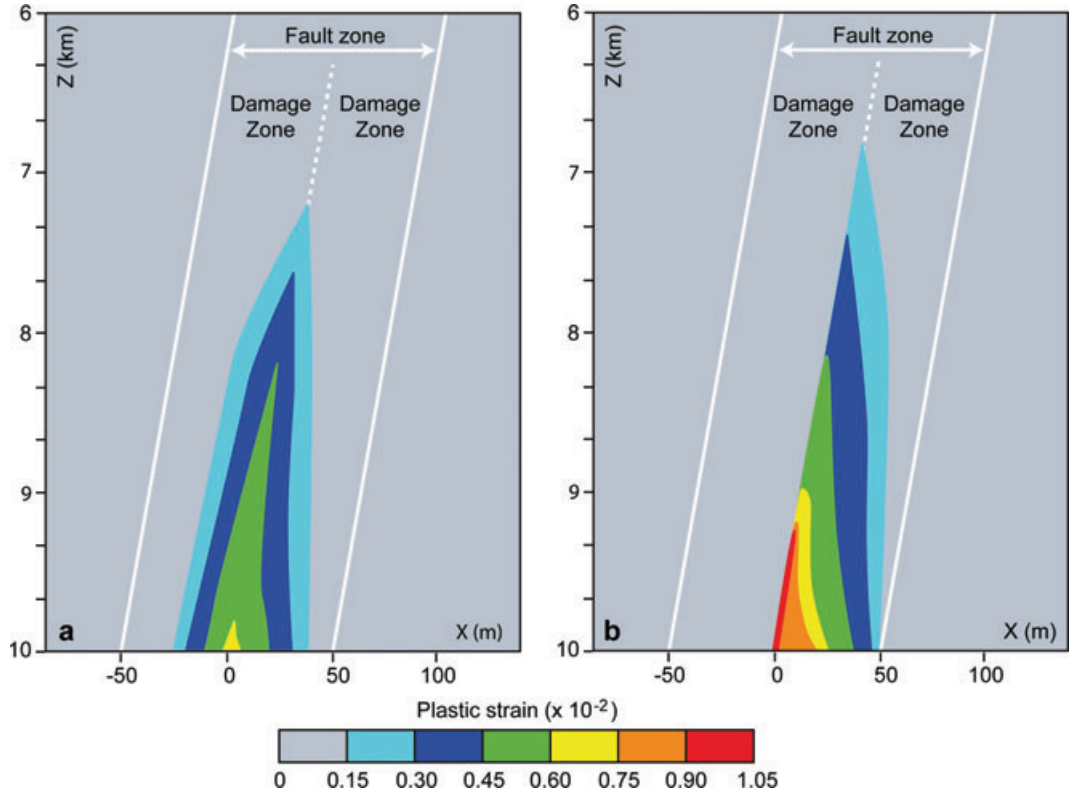

Figure 6. (a, b) Distribution of the permanent plastic shear strain along the fault zone for case 1 in (a) and case 2 in (b) ($t = 1.5$ d). Note that the plastic shear strain is higher in the most permeable side of the fault zone (1.05×10^{-2}). A model with a symmetrical distribution of fault zone properties produces a plasticized shear zone with a maximum strain of 6.03×10^{-3}. A sufficiently large permeability contrast in the fault zone produces a larger amount of plasticized shear zone and can rupture the damage zone completely near the pressure source.

behaviour of the PSZ where earthquakes can nucleate. The slip process varies along the fault depending on the spatial variations of hydromechanical properties and the fluid and stress transfer which reduce the fault strength. In contrast to fluid flow in homogeneous media, fluid flow along a heterogeneous fault zone generates asymmetric stress changes and ruptures. Consequently, our results show that a contrast of hydromechanical properties across a fault may cause fluid flow and rupture to occur in a preferred direction. This could in turn explain why some earthquakes propagate in a preferred direction; why the distribution of slip is sometimes heterogeneous, with patches of high and low slip; and, also, the dissipation of a fraction of the earthquake energy and coseismic dilatancy around the zones of slip (Ben Zion & Sammis 2003; Manighetti *et al.* 2005; Fielding *et al.* 2009).

4.2 Plastic strain off the PSZ and dimension of the ruptured volume

Results confirm that rupture along faults does not solely affect a single planar surface, but also a broad volume around that surface. This is consistent with several recent geological and seismological observations of faults structure that found asymmetric damage zones that can reach several hundreds metres in thickness (Chester *et al.* 2004; Dor *et al.* 2005; Lewis *et al.* 2005, 2007). Our simulations showed that on faults with hydromechanical heterogeneities at the scale of the internal structure, the fluid pressure and rupture are highly asymmetric. Thus, our results provide a new context for inferring from geological observations of fault zone damage a possible preferred propagation direction of ruptures and fluid flux along faults.

It is known that the reduction or increase in the amount of plastic strain off the slip zone affects the rupture propagation and speed, as well as the slip gradient (Andrews 2005; Templeton & Rice 2008; Viesca *et al.* 2008). The results of Fig. 7 show that the location, spatial extent and magnitude of plastic strain are sensitive to the permeability and rigidity contrast. The lower permeability and rigidity contrasts are, the lower the magnitude of plastic strain is, but larger is the ruptured area. The net effect of the permeability contrast (Fig. 7d) is the localization of plastic strain in a preferred direction, that of rupture predominantly in the more permeable side of the fault. Thus, the above-mentioned considerations suggest that earthquake faults may likely experience different patterns of off-fault plastic straining associated with the presence of fluids.

4.3 Comparison with observations in other studies

Our results are in agreement with previous works by Rudnicki & Rice (2006) and Dunham & Rice (2008) who have studied fault slip between fluid-saturated materials that are elastically identical but have dissimilarity in poroelastic properties, within damage zones along the fault walls. They demonstrated in the context of spontaneously propagating ruptures that a fault zone in which there is a contrast of properties, the evolution of rupture and the pore pressure increase and decrease respectively on the compressional and extensional sides of the rupture tip. In particular, the pore pressure change would depend on the permeabilities and storage coefficients on the compressional and extensional side of the fault. Moreover, a rupture

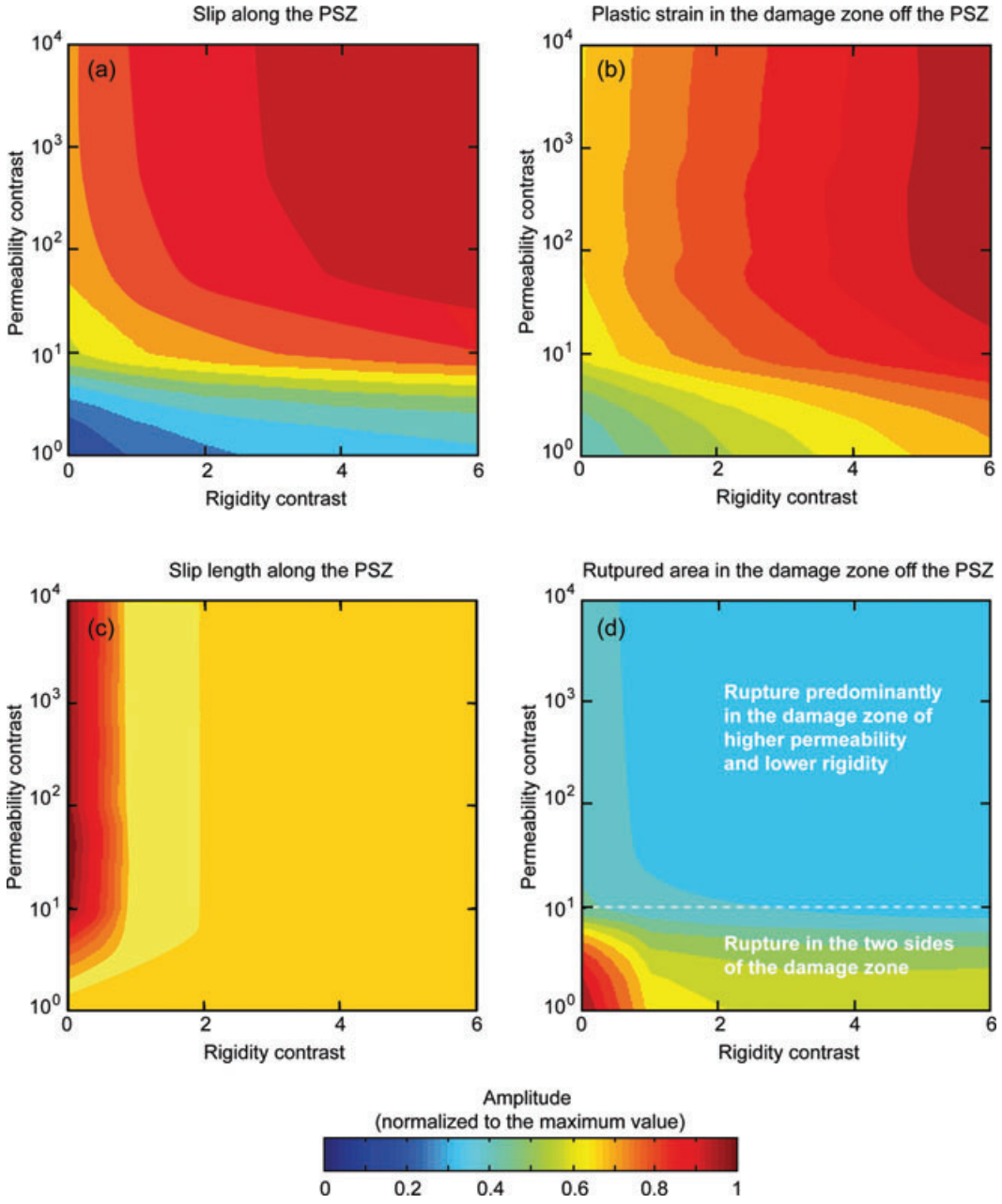

Figure 7. Phase diagrams illustrating the effects of the contrast of permeability and rigidity inside the fault zone on (a) the slip measured along the PSZ, (b) the plastic strain off the PSZ inside the surrounding damage zone, (c) the slip length along the PSZ, and (d) the ruptured area off the PSZ inside the damage zone. Effect of the rigidity contrast (the range E = 10–70 GPa; $0 < \gamma < 6$), and the permeability contrast (the range $k = 1 \times 10^{-18}$ m^2 to 1×10^{-14} m^2; $0 < \gamma < 10^4$).

through a fault with more permeable material on the compressional side of the fault than on the extensional side would induce a net pore pressure increase on the fault, favouring further instability and rupture. Thus, the poroelastic response can cause either reductions of or increase in effective normal stress, depending on which side of the fault is more compliant and/or more permeable. This effect is enhanced if the compliant side is more permeable, and is reduced each other if the stiff side is more permeable. Since the effective normal stress change is different on either side of the slip zone, the material contrast introduces asymmetry into the off-fault rupture process. Our results are also compatible with works of Viesca *et al.* (2008). Plastic strain off the slip zone is larger in the direction in which the largest increases in pore pressure strongly decrease the effective normal stress and weaken the rock. Thus, plastic strain is enhanced in the more compliant and permeable side, and reduced or absent in the stiff and low-permeable side. Nevertheless, these results differ from models with spontaneous generation of off-fault damage to in-plane ruptures along material interface, neglecting the effect of fluids (Ben-Zion & Shi 2005). Indeed, Ben-Zion & Shi (2005) showed that plastic strain is generated primarily on the stiffer side of the fault zone and the off-fault damage is significant for conditions that correspond to the top few kilometres (top 5 km) of the crust. These results are compatible with field observations of shallow asymmetric damage patterns (Dor *et al.* 2006a,b) and seismological imaging studies (Ben-Zion *et al.* 2003; Peng *et al.* 2003; Lewis *et al.* 2005, 2007) in the structure of several large faults.

5 CONCLUSION

Our model presents an interpretation of the physical processes controlling fault slip and distributed plastic deformation within the nearby damage zone. We examined the possibility that earthquakes could also be triggered by transient pulses of high-fluid pressure imposed in a limited source region at the base of the brittle upper crust. We performed a systematic parameter-space study of rupture properties on a fault zone with heterogeneous permeability and Young's modulus. We found that both fluid flow and hydromechanical deformation cause property changes in the fault zone and, through variations in fluid pressure and stress, subsequent changes in the fault strength. We also found that the properties contrast significantly changes the amount of slip along the fault and plastic strain off the fault, and consequently, the degree of rupture asymmetry. This asymmetry is manifested by larger off-fault plasticity in the less rigid and more permeable side of the fault. Nevertheless, several studies (Rice 2006; Sone & Shimamoto 2009) have shown correlations with other factors not considered in the numerical experiments presented here, and that may significantly affect fault strength. These include the role of fault friction—which depends on the extent of slip, rate of slip and slip history, shear heating and melting of fault materials under high compression. These mechanisms may interact and result in complex seismic or aseismic slip behaviours. Further investigation coupling the hydromechanical heterogeneities of fault zones with friction laws is a high priority to better understand earthquake ruptures. It is important to clarify such effects, and to test the predictions associated with ruptures with laboratory and field observations.

While the cases addressed in this paper are for a fault zone initially at hydrostatic fluid pressure before the sudden high-pressure loading, the model can be applied to the study of rupture on a critically stressed fault in the presence of fluid pressures in excess of hydrostatic (i.e. near-lithostatic) at the initial state. Along such faults, very small stress perturbations (few tens of kPa) may facilitate triggering of earthquakes, slow-slip events and non-volcanic tremors (Miyazawa & Mori 2006; Rubinstein *et al.* 2007; Cappa *et al.* 2009; Taira *et al.* 2009; Thomas *et al.* 2009).

Finally, this work presents constraints on the role of fluids in rupturing faults separating two different media with spatially variable material properties—conditions that are representative of natural fault zones. Our results suggest that the structural evolution of such faults may be linked with the hydromechanical properties of the damage zone, highlighting the interaction between hydraulic diffusivity and stress transfer. During a high-fluid pressure event, fault zones may tend to develop local fluid overpressures and stresses in discrete patches that weaken the fault strength to a level below the prevailing shear stress. Thus, a consequence of rupture on a fault with contrasted properties could be the result of a heterogeneous spatial earthquake distribution and coseismic deformation through volume rather than a single ruptured plane. We suggest that introducing heterogeneities in hydromechanical properties, and plastic deformation in a volume around the faults in rupture models can be a way to improve the quantitative interpretation of earthquake observations.

ACKNOWLEDGMENTS

This work was financially supported by University of Nice Sophia-Antipolis (BQR 2009) and Côte d'Azur Observatory (BQR 2010). I thank Olivier Fabbri for his constructive comments that substantially improved a first version of the manuscript. I also thank the associate editor, Yehuda Ben-Zion, and two anonymous reviewers for their insightful comments and valuable suggestions.

REFERENCES

Andrews, D.J., 2002. A fault constitutive relation accounting for thermal pressurization of pore fluid, *J. geophys. Res.,* **107**(B12), 2363, doi:10.1029/2002JB001942.

Andrews, D.J., 2005. Rupture dynamics with energy loss outside the slip zone, *J. geophys. Res.,* **81,** 5679–5687.

Becken, M., Ritter, O., Park, S., Bedrosian, P.A., Weckmann, U. & Weber, M., 2008. A deep crustal fluid channel into the San Andreas Fault system near Parkfield, California, *Geophys. J. Int.,* **173,** 718–732, doi:10.1111/j.1365-246X.2008.03754.x.

Ben-Zion, Y. & Sammis, C.G., 2003. Characterization of fault zones, *Pure appl. Geophys.,* **160,** 677–715.

Ben-Zion, Y. & Shi, Z., 2005. Dynamic rupture on a material interface with spontaneous generation of plastic strain in the bulk, *Earth planet. Sci. Lett.,* **236,** 486–496.

Ben-Zion, Y. *et al.,* 2003. A shallow fault zone structure illuminated by trapped waves in the Karadere-Duzce branch of the North Anatolian fault, western Turkey, *Geophys. J. Int.,* **152,** 699–717.

Brietzke, G.B. & Ben-Zion, Y., 2006. Examining tendencies of in-plane rupture to migrate to material interfaces, *Geophys. J. Int.,* **167,** 807–819, doi:10.1111/j.1365-246X.2006.03137.x.

Cappa, F., 2009. Modeling fluid transfer and slip in a fault zone with heterogeneous hydromechanical properties in its internal structure, *Geophys. J. Int.,* **178,** 1357–1362, doi:10.1111/j.1365-246X.969.2009.04291.x.

Cappa, F., Guglielmi, Y. & Virieux, J., 2007. Stress and fluid transfer in a fault zone due to overpressures in the seismogenic crust, *Geophys. Res. Lett.,* **34,** L05301, doi:10.1029/2006GL028980.

Cappa, F., Rutqvist, J. & Yamamoto, K., 2009. Modeling crustal deformation and rupture processes related to upwelling of deep CO_2-rich fluids during the 1965–1967 Matsushiro earthquake swarm in Japan, *J. geophys. Res.,* **114,** B10304, doi:10.1029/2009JB006398.

Chester, F.M., Chester, J.S., Kirschner, D.L., Schulz, S.E. & Evans, J.P., 2004. Structure of large-displacement, strike-slip fault zones in the brittle continental crust, in *Rheology and Deformation in the Lithosphere at Continental Margins,* eds Karner, G.D., Taylor, B., Driscoll, N.W. & Kohlstedt, D.L., Columbia University Press, New York, NY.

Dor, O., Rockwell, T.K. & Ben-Zion, Y., 2006a. Geological observations of damage asymmetry in the structure of the San Jacinto, San Andreas and Punchbowl faults in Southern California: a possible indicator for preferred rupture propagation direction, *Pure appl. Geophys.,* **163,** 301–349, doi:10.1007/s00024-005-0023-9.

Dor, O., Ben-Zion, Y., Rockwell, T.K. & Brune, J., 2006b. Pulverized rocks in the Mojave section of the San Andreas fault zone, *Earth planet. Sci. Lett.,* **245,** 642–654, doi:10.1016/j.epsl.2006.03.034.

Dunham, E. & Rice, J.R., 2008. Earthquake slip between dissimilar poroelastic materials, *J. geophys. Res.,* **113,** B09304, doi:10.1029/2007JB005405.

Faulkner, D.R. & Rutter, E.H., 1998. The gas permeability of clay-bearing fault gouge at 20°C, in *Faults, Fault Sealing and Fluid Flow in Hydrocarbon Reservoirs,* Geol. Soc. Spec. Pub. Vol. 147, pp. 147–156, eds Jones, G., Fisher, Q. & Knipe, R.J., Geological Society, London, doi:10.1144/GL.SP.1998.147.01.10.

Faulkner, D.R., Mitchell, T.M., Healy, D. & Heap, M., 2006. Slip on 'weak' faults by the rotation of regional stress in the fracture damage zone, *Nature,* **444**(7121), 922–925.

Fielding, E.J., Lundgren, P., Bürgmann, R., Funning, G.J., 2009. Shallow fault-zone dilatancy recovery after the 2003 Bam earthquake in Iran, *Nature,* **458,** 64–68, doi:10.1038/nature07817.

Fulton, P. M. & Saffer, D. M., 2009. Potential role of mantle-derived fluids in weakening the San Andreas Fault, *J. geophys. Res.,* **114,** B07408, doi:10.1029/2008JB006087.

Gudmundsson, A., 2004. Effects of Young's modulus on fault displacement, *C.R. Geosci.,* **336,** 85–92.

Gudmundsson, A., Simmenes, T.H., Larsen, B. & Philipp, S.L., 2010. Effects of internal structure and local stresses on fracture propagation,

deflection, and arrest in fault zones, *J. Struct. Geol.,* **32,** 1643–1655, doi:10.1016/j.jsg.2009.08.013.

Guglielmi, Y., Cappa, F. & Amitrano, D., 2008. High-definition analysis of fluid-induced seismicity related to the mesoscale hydromechanical properties of a fault zone, *Geophys. Res. Lett.,* **35,** L06306, doi:10.1029/2007GL033087.

Hickman, S., Zoback, M. & Ellsworth, W., 2004. Introduction to special section: preparing for the San Andreas Fault Observatory at Depth, *Geophys. Res. Lett.,* **31,** L12S01, doi:10.1029/2004GL020688.

Lewis, M.A., Peng, Z., Ben-Zion, Y. & Vernon, F.L., 2005. Shallow seismic trapping structure in the San Jacinto fault zone near Anza, California, *Geophys. J. Int.,* **162,** 867–881, doi:10.1111/j.1365-246X.2005.02684.x.

Lewis, M.A., Ben-Zion, Y. & McGuire J.J., 2007. Imaging the deep structure of the San Andreas fault south of Hollister with joint analysis of fault zone head and direct P arrivals, *Geophys. J. Int.,* **169,** 1028–1042, doi:10.1111/j.1365-246X.2006.03319.x.

Manga, M. & Wang, C.Y. 2007. Earthquake hydrology, in *Treatise on Geophysics,* Vol. 4, pp. 293–320, ed. Schubert, G., Elsevier, San Diego, CA.

Manighetti, I., Campillo, M., Sammis, C., Mai, P.M. & King G., 2005. Evidence for self-similar, triangular slip distributions on earthquakes: implications for earthquake and fault mechanics, *J. geophys. Res.,* **110,** B05302, doi:10.1029/2004JB003174.

Miller, S.A., Collettini, C., Chiaraluce, L., Cocco, M., Barchi, M. & Kaus, B.J.P., 2004. Aftershocks driven by a high-pressure CO_2 source at depth, *Nature,* **427**(6976), 724–727.

Mitchell, T.M. & Faulkner, D.R., 2009. The nature and origin of off-fault damage surrounding strike-slip fault zones with a wide range of displacements: a field study from the Atacama fault system, northern Chile, *J. Struct. Geol.,* **31**(8), 802–816, doi:10.1016/j.jsg.2009.05.002.

Miyazawa, M. & Mori, J., 2006. Evidence suggesting fluid flow beneath Japan due to periodic seismic triggering from the 2004 Sumatra-Andaman earthquake, *Geophys. Res. Lett.,* **33,** L05303, doi:10.129/2005GL025087.

Noda, H. & Shimamoto, T., 2005. Thermal pressurization and slip-weakening distance of a fault: an example of the Hanaore fault, southwest Japan, *Bull. seism. Soc. Am.,* **95**(4), 1224–1233.

Peng, Z., Ben-Zion, Y., Michael, A.J. & Zhu, L., 2003. Quantitative analysis of seismic trapped waves in the rupture zone of the 1992 Landers, California earthquake: evidence for a shallow trapping structure, *Geophys. J. Int.* **155,** 1021–1041.

Rice, J. R., 2006. Heating and weakening of faults during earthquake slip, *J. geophys. Res.,* **111,** B05311, doi:10.1029/2005JB004006.

Rudnicki, J.W. & J.R. Rice, 1975. Conditions for localization of deformation in pressure-sensitive dilatant materials, *J. Mech. Phys. Solids,* **23,** 371–394.

Rudnicki, J.W. & J.R. Rice, 2006. Effective normal stress altération due to pore pressure changes induced by dynamic slip propagation on a plane between dissimilar materials, *J. geophys. Res.,* **111,** B10308, doi:10.1029/2006JB004396.

Rubinstein, J.L., Vidale, J.E., Gomberg, J., Bodin, P., Creager, K.C. & Malone S.D., 2007. Non-volcanic tremor driven by large transient shear stresses, *Nature,* **448**(2), 579–582, doi:10.1038/nature06017.

Scholz, C.H., 2002. *The Mechanics of Earthquakes and Faulting,* p. 471, 2nd edn., Cambridge University Press, Cambridge.

Shi, Z. & Ben-Zion, Y., 2006. Dynamic rupture on a bimaterial interface governed by slip-weakening friction, *Geophys. J. Int.,* **165,** 469–484, doi:10.1111/j.1365-246X.2006.02853.x.

Sibson, R.H., 1973. Interactions between temperature and pore fluid pressure during earthquake faulting: a mechanism for partial or total stress relief, *Nature Phys. Sci.,* **243,** 66–68.

Sibson, R.H., 2003. Thickness of the seismic slip zone, *Bull. seism. Soc. Am.,* **93**(3),1169–1178.

Sone, H. & Shimamoto, T., 2009. Frictional resistance of faults during accelerating and decelerating earthquake slip, *Nat. Geosci.,* **2,** 705–708, doi:10.1038/NGEO637.

Taira, T., Silver, P.G., Niu, F. & Nadeau, R.M., 2009. Remote triggering of fault-strength changes on the San Andreas fault at Parkfield, *Nature,* **461**(1), 636–639, doi:10.1038/nature08395.

Templeton, E.L. & Rice J.R., 2008. Off-fault plasticity and earthquake rupture dynamics: 1. Dry materials or neglect of fluid pressure changes, *J. geophys. Res.,* **13**(B9), B09306, doi:10.1029/2007JB005529.

Thomas, A.M., Nadeau, R.M. & Bürgmann R., 2009. Tremor-tide correlations and near-lithostatic pore pressure on the deep San Andreas fault, *Nature,* **462**(24), 1048–1051, doi:10.1038/nature08654.

Vermilye, J.M. & Scholz, C.H., 1998. The process zone: a microstructural view of fault growth, *J. geophys. Res.,* **103**(B6), 12 223–12 237.

Viesca, R.C., Templeton E.L. & Rice J.R., 2008. Off-fault plasticity and earthquake rupture dynamics: 2. Effects of fluid saturation, *J. geophys. Res.,* **113,** B09307, doi:10.1029/2007JB005530.

Wannamaker, P.E., *et al*. 2009. Fluid and deformation regime of an advancing subduction system at Martlborough, New Zealand, *Nature,* **460,** 733–737, doi:10.1038/nature08204.

Wibberley, C.A.J & Shimamoto, T., 2003. Internal structure and permeability of major strike-slip fault zones: the Median Tectonic Line in Mie Prefecture, Southwest Japan, *J. Struct. Geol.,* **25,** 59–78.

Wibberley, C.A.J & Shimamoto, T., 2005. Earthquake slip weakening and asperities explained by fluid pressurization, *Nature,* **436,** 689–692, doi:10.1038/nature03901.

Wilson, J.E., Chester, J.S. & Chester, F.M., 2003. Microfracture analysis of fault growth and wear processes, Punchbowl Fault, San Andreas System, California, *J. Struct. Geol.,* **25**(11), 1855–1873.

APPENDIX: THE FIELD EQUATIONS AND MODEL PARAMETERS

In the models, fluid flow is simulated by solving the diffusion equation with spatially variable hydraulic parameters in a poroelastoplastic medium

$$\nabla.\left(\frac{k}{\mu}\left(\nabla P-\rho_f g\right)\right)+\frac{\partial m}{\partial t}=0, \tag{A1}$$

where k is the permeability (m^2), ϕ is the porosity, μ is the fluid viscosity (10^{-3} Pa s) P is fluid pressure (Pa), ρ_f is the fluid density (1000 kg m^{-3}), g is the gravitational acceleration directed downward (9.81 m s^{-2}), t is the time (s) and the rate of changes in fluid mass (m) is defined as function of the elastic deformation and plastic dilatancy as follows

$$\partial m=\rho_f\left(\frac{\alpha}{KB}\right)\left(\partial P+B\frac{\partial\sigma_{kk}}{3}\right)+\rho_f\partial\varepsilon^p, \tag{A2}$$

where α is the Biot's coefficient ($\alpha=1-K/K_s$), K is the drained Bulk modulus of the porous material, K_s is the Bulk modulus of the solid skeleton, B is the Skempton's coefficient expressed as

$$B=\frac{\alpha}{1-(1+\phi_0)\frac{K}{K_s}+\frac{\phi_0 K}{K_f}} \tag{A3}$$

with K_f the fluid Bulk modulus.

In the model, the porosity (ϕ) and the permeability (k) vary with the depth and the total volumetric strain (ε_v)

$$\phi=1-\left(1-\left(\phi_0 e^{-\frac{z}{\beta}}\right)\right)e^{-\varepsilon_v} \tag{A4}$$

$$k=\left(k_0 e^{-\frac{z}{\beta}}\right)\left(\frac{\phi}{\phi_0 e^{-\frac{z}{\beta}}}\right)^n, \tag{A5}$$

where ϕ_0 is the porosity at zero stress, k_0 is the permeability at zero stress, n is a porosity sensitivity exponent (n = 3), β is a depth sensitivity parameter ($\beta=2600$) and z is the depth. The initial porosity and permeability distribution decreases exponentially with depth assuming a difference of two orders of magnitude between the ground surface and the base of the seismogenic crust at

10 km depth. The volumetric strain is defined as the sum of the elastic ($d\varepsilon^e$) and plastic ($d\varepsilon^p$) components of strain (Rudnicki & Rice 1975)

$$d\varepsilon_v = d\varepsilon^e + d\varepsilon^p = \frac{d\sigma}{K} + \frac{\psi}{h}\left(d\tilde{\tau} + \mu_s d\sigma'_{ij}\right) \tag{A6}$$

where σ'_{ij} is the Therzaghi effective stress (positive for tension, negative for compression), $\tilde{\tau}$ is the second invariant of the deviatoric stress tensor ($\tilde{\tau} = \sqrt{(1/2)s_{ij}s_{ij}}$), Ψ is the dilation angle and μ_s is the coefficient of static friction. In the results shown here, we considered an ideally plastic response assuming that ($d\tau + \mu_s d\sigma$) and the plastic hardening modulus (h) vanish such that their limit exists as a positive quantity corresponding to the plastic strain increment (Rudnicki & Rice 1975). The appropriate effective stress (σ'_{ij}) measure for evaluating strain increments is calculated from the Terzaghi's effective stress equation

$$\sigma'_{ij} = \sigma_{ij} - \alpha P \delta_{ij}, \tag{A7}$$

where δ_{ij} is the Kronecker delta.

If fluid pressure increases in the PSZ of the fault and the fractured rock volume that surrounds it, the effective normal stress across the fault will decrease; this effect in turn will reduce the fault strength according to the Coulomb failure criterion

$$\tau = c + \mu_s \sigma'_n \tag{A8}$$

where τ is the driving shear stress for seismogenic fault slip, c is the cohesion and σ'_n is the effective normal stress.

Our model is fully coupled with a two-way coupling: (1) fluid-to-solid and (2) solid-to-fluid. The numerical experiments were solved with the finite-difference method. The numerical grid was refined near the fault zone, with grid sizes gradually increasing towards the lateral model boundaries. Vertical resolution is 25 m. *In situ* and boundary fluid pressures were considered to be hydrostatic (Fig. 3). On the top boundary, the ground surface is free to move, whereas stress at other boundaries follows the lithostatic gradient. Temperature is assumed to follow a constant geothermal gradient with depth (30 $^\circ$C km^{-1}). After computing the initial state, we applied instantaneously a pressurization (i.e. pressure pulse) corresponding to the lithostatic pressure (i.e. $P \sim 0.29$ GPa) at 10 km depth at the base of the fault zone. Consequently, the fluid pressure in the fault tends to increase due to the fluid mass transfer from the deep lithostatically overpressured zones to the shallow ones where fluids are at hydrostatic pressure. Potential high-fluid pressure sources at such depths may be initiated by accumulation of sea water, meteoric water, CO_2 degassing or minerals dehydration from the mantle or the lower crust (Manga & Wang 2007). Another alternative for the initiation of such high-fluid pressures can be the coseismic release of fluids trapped at depth (Miller *et al.* 2004). This can occur when earthquake rupturing of low permeability seals release previously trapped high-pressure fluids in reservoirs. Then, large fluxes of fluid can propagate through a fault fracture network created during the main shock as a pressure pulse.

For the sake of simplicity, we will consider that the permeability and porosity will change significantly in the x–z plane during the pressurization. This approximation is the main limit of the model; indeed, permeability and porosity should also vary in the third dimension (i.e. along-strike direction) according to common geological models of fault structure.